Available online at www.sciencedirect.com
SCIENCE DIRECT
Journal of Power Sources 158 (2006) 591–599
JOURNAL OF POWER SOURCES
www.elsevier.com/locate/jpowsour

Analysis of the passive surface film on a graphite electrode charged in polysiloxane-based electrolyte

Hiroshi Nakahara [a,*], Sang-Young Yoon [a], Tracy Piao [a], Florian Mansfeld [b], Steven Nutt [b]

[a] *Quallion LLC, Sylmar Biomedical Park, 12744 San Fernando Rd., Sylmar, CA 91342, USA*
[b] *Department of Material Science and Engineering, University of Southern California, Los Angeles, CA 90089-0241, USA*

Received 7 September 2005; received in revised form 23 September 2005; accepted 26 September 2005
Available online 8 November 2005

Abstract

In this study, electrochemical impedance spectroscopy (EIS) was performed during the first charge of a graphite/lithium metal test cell. The graphite electrode was separated from the lithium metal electrode by a porous polyethylene membrane maintaining polysiloxane-based electrolyte with the dissolved lithium bis(oxalato)borate (LiBOB). Analysis of the EIS data indicated that films with distinct electrical properties were present on the graphite surface. The value of each component in the equivalent circuit used in the data analysis depended on the cell voltage. The magnitude of the resistance and capacitance of the surface films changed at 1.8 V and 1.4 V, and the magnitude of the charge transfer resistance and double-layer capacitance changed at ∼1.8 V. The results of the EIS analysis correlated with the observed morphological changes of the graphite surface, which included formation of an island-like film and a gel-like film, as reported previously [H. Nakahara, A. Masias, S.Y. Yoon, T. Koike, K. Takeya, Proceedings of the 41st Power Sources Conference in Philadelphia, 14–17 June, 2004, p. 165].

Keywords: Lithium battery; Graphite; Polymer electrolyte; Siloxane; LiBOB; Passive film

1. Introduction

Extensive investigations have been conducted on the formation of the solid electrolyte interface (SEI) on graphite electrode surfaces in non-aqueous electrolytes, such as the ethylene carbonate/diethyl carbonate system [2,3]. In these reports, the authors determined that exfoliation of graphene layers occurred during initial charging in propylene carbonate-based electrolytes because of co-intercalation of solvent [2,4]. Earlier studies asserted that the SEI film formed mainly by a solvent decomposition reaction, and that it was composed of $ROCO_2Li$ species, Li_2CO_3, and LiF [5–8]. Other investigators concluded that the novel lithium salt lithium bis(oxalato)borate (LiBOB) forms an SEI film directly on graphite rather than by a solvent decomposition reaction [9–11]. More recent studies have indicated that polysiloxane may be a suitable electrolyte in a lithium battery system because of the high conductivity relative to other polymer materials [12–15]. For example, polyethylene oxide (PEO) is a well-known solid polymer electrolyte that shows conductivity in the range of 10^{-6} S cm^{-1} to 10^{-7} S cm^{-1} [16]. The conductivity of polysiloxane-based electrolyte exceeds that of PEO by several orders of magnitude, having a value of approximately 10^{-3} S cm^{-1} [17].

Polysiloxane-based electrolyte has become a primary candidate for the development of large-size lithium batteries for applications, such as electric vehicles, in which safety is a prime consideration [16]. Despite numerous reports of SEI film formation in conventional electrolyte, there have been few studies of the SEI formation in polysiloxane-based electrolyte aside from our previous report [1] in which the existence of two different types of passive film and their associated morphological features was revealed by SEM observations. One type of passive film was island-like and formed directly on the graphite surface, while the other was a gel-like film covering the island-like film. To reduce the capacity loss and increase the discharge capacity of the graphite electrode, it was necessary to prevent the formation of the gel-like film. The electrochemical nature of these films has not been clarified yet.

Electrochemical impedance spectroscopy (EIS) is a powerful tool to investigate electrolyte-electrode interface reactions

* Corresponding author. Tel.: +1 818 833 2000; fax: +1 818 833 2001.
E-mail address: hiroshi@quallion.com (H. Nakahara).

0378-7753/$ – see front matter © 2005 Elsevier B.V. All rights reserved.
doi:10.1016/j.jpowsour.2005.09.041

[18–26]. EIS has been applied to the analysis of the electrochemical lithium intercalation reaction into carbonaceous material in the carbonate electrolyte system and the subsequent formation of a SEI film [27–33]. While EIS data are commonly plotted in complex plane plots ($-Z''$ versus Z'), the dependence of the impedance on the frequency of the applied signal can be better understood in Bode plots.

For the electrochemical process of lithium intercalation into carbonaceous material, a series of semicircles in the high- or middle-frequency regions is normally observed in the complex plot, followed by a straight line in the low-frequency region. The semicircles are normally attributed to the migration of lithium ions through the SEI film, the electric double-layer capacitive phenomena, and the charge transfer reaction on the surface of the carbonaceous material. The straight line following the semicircles corresponds to lithium diffusion through the SEI layer or the graphene layer of the carbonaceous material. The conductivity of the electrolyte can be obtained from the highest frequency region in complex plots.

Most EIS analysis relating to lithium intercalation with carbonaceous material has been carried out with conventional carbonate electrolyte systems. In these analyses, various equivalent circuits (EC) are proposed for the electrochemical reactions involved. These ECs afford insight and provide understanding of the electrochemical properties in those reactions. For polymeric electrolyte systems, several reports have described conductivity calculations using EIS data. However, few investigators have attempted to use EIS to interpret electrochemical reactions especially the formation of the SEI film [27,31,34].

In this study, EIS measurements were performed while charging the graphite electrode with polysiloxane-based electrolyte containing dissolved LiBOB salt. The objective was to gain understanding of the electrochemical characteristics of island-like and gel-like films and to clarify the rate-limiting process in the electrochemical reactions occurring during intercalation of lithium with the graphite electrode in the presence of a polysiloxane-based electrolyte. An EC was proposed for the analysis of the measured impedance spectrum. The dependences of the resistance and capacitance of the passive films, the electric double-layer capacitance and the charge transfer resistance of lithium on the cell voltage were determined. Furthermore, the relationship between the proposed EC and the morphological and compositional properties of the two different passive films on the graphite surface was evaluated [1].

2. Experimental approach

2.1. Electrode morphology and composition

The molecular structure of poly(dimethyl)siloxane poly(ethylene oxide) investigated in this study is shown in Fig. 1. In the present experiments, the molecule indexed at $m = 0$, $n = 8$, and $x = 3$ was used. Lithium bis(oxalato)borate (LiBOB, Chemetall GmbH), was dissolved in poly(dimethyl)siloxane poly(ethylene oxide) to achieve a 0.8 M concentration for testing. The electrolyte was a liquid at room temperature.

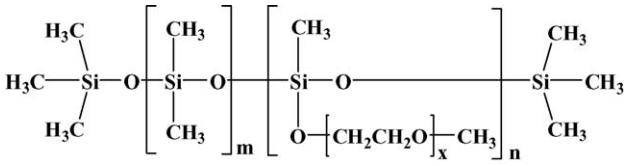

Fig. 1. Molecular structure of poly(dimethyl)siloxane poly(ethylene oxide).

A polysiloxane-based electrolyte with the dissolved LiBOB was used to modify the surface of highly oriented pyrolytic graphite (HOPG). A block of HOPG (2 mm × 2 mm × 1 mm) was used as the working electrode. Copper mesh was wrapped around the HOPG block electrode used as a current collector. The electrode was covered with a polyethylene porous separator, and lithium metal was pressed against a copper mesh and used as the counter electrode. The working electrode, counter electrode, separator, and electrolyte were packaged in a heat-sealed aluminum laminated bag. The seven laminated cells were charged to the prescribed voltages (2.0 V, 1.8 V, 1.7 V, 1.6 V, 1.4 V, 1.0 V, and 0.02 V, respectively). The charged electrode were removed from the disassembled cell in a glove box filled with Ar gas, maintaining the dew-point below −75 °C, rinsed with diethyl carbonate (DEC), and dried under vacuum at room temperature. The surfaces of the HOPG were observed by SEM (JEOL JSM-5910LV) after sputter-coating with gold. In addition, compositional analysis of the HOPG surfaces was performed by Auger electron spectroscopy (AES; PHI 660 Scanning Auger Microprobe) with Ar sputtering.

2.2. Electrochemical spectroscopy

The graphite electrodes were prepared by mixing 33.6 g of mesocarbon microbeads (Osaka Gas Co., Ltd., MCMB 25–28), 14.4 g of graphite fiber (Petoca Co., Ltd., GMCF), 62.6 g of 2 wt% aqueous solution of carboxymethyl cellulose (Dai-ichi Kogyo Seiyaku Co., Ltd., Celogen WSC), and 1.88 g of a 40% aqueous dispersion of styrene butadiene rubber (Dai-ichi Kogyo Seiyaku Co., Ltd., BM-400) in a mixer. The mixture was spread on a copper foil (10 μm thick) with a doctor blade and dried in an oven at 80 °C. The dried electrode plate was then pressed using a roll press to a thickness of 102 μm. Pressed electrodes were dried in a vacuum oven at 120 °C for 12 h. The carbonaceous electrodes (15 mm in diameter) were punched out of the dried electrode plate. Lithium metal electrodes (16 mm in diameter) were punched from a lithium metal sheet (Honjo metal, 100 μm thick). Coin cells (2032-type) were prepared by stacking a lithium metal electrode, a separator, a carbonaceous electrode, spacer disks made from stainless steel, and a spring in sequence. The separator was a 25 μm thick polyethylene porous membrane (Tonen Chemical Co., Ltd.). The test cell was filled with the polysiloxane-based electrolyte. All parts used for the coin cell assembly were dried in a vacuum oven at 60 °C for more than 8 h.

Impedance measurements were performed with a potentiostat (Solartron, SI1287) and a transfer function analyzer (Solartron, 1255B). The frequency used for the impedance measurements was 0.1 Hz–500 kHz and the signal amplitude was 10 mV. Poten-

tial step coulometry was performed with an electrochemical interface (Solartron, SI1287). Impedance spectra were measured after the cell had been charged at a rate of C/200 to the prescribed voltage and maintained at that voltage for 24 h. The voltage was then stepped to the next potential, and the procedure was repeated. In this manner, the cell was charged from the initial open-circuit voltage (OCV) after assembling a 2032 type cell comprised with lithium metal counter and reference electrode down to 0.05 V at 25 °C.

The impedance data were analyzed using commercial software (Scribner Associates, Inc., Zview™) that included a batch fitting function that performed fitting for multiple sets of impedance spectra step-by-step. In this method, initial values of the fit parameter were obtained from values fitted in the previous step. These values were obtained for a set of measured impedance spectra, from which a complex plane plot was generated at a higher voltage. Next, the fitted parameters generated in one step were used as initial values to fit the spectra for the subsequent step. These procedures were repeated in successive steps until the values of the parameters fitted converged [35]. The conductivity of electrolyte was calculated using the real part of the impedance obtained in the high-frequency region of the complex plane plot.

3. Implementation of equivalent circuit model

EIS data for lithium ion cells and lithium metal cells have been reported extensively [19–21,23,36]. In related work, logic diagrams and ECs have been proposed for cells with a graphite/lithium metal configuration [37–42]. In most of these studies, an *R*–*C* parallel or *R*–CPE parallel circuit was used to describe the presence of a surface film layer on the electrode [37,39–43]. The EC used in these reports can be divided into three segments corresponding to the frequency regions in a complex plane plot [27,30,31,40,44]. The segments include (a) electric connection resistance and the electrolyte bulk resistance corresponding to the resistance at the highest frequencies, followed by (b) a *R*–*C* parallel circuit describing the SEI layer in the mid-frequency region, and finally, (c) a *R*–*C* parallel circuit for double-layer capacitance and charge transfer reaction, including a Warburg diffusion term in the low-frequency region corresponding to lithium diffusion in the solid state, as shown in Fig. 2.

In general, because semicircles often tend to be depressed in a complex plane plot due to electrode geometry, a constant phase element (CPE) is used in an EC for the porous electrode evaluated in the present study. The use of a CPE is justified because of the geometrical effect on capacitance in electrochemical reactions [45–47]. The complex impedance of a CPE, Z_{CPE}, is expressed by:

$$Z_{CPE} = \frac{1}{\left[T \cdot (j \cdot \omega)^P\right]}, \quad (1)$$

where T represents the pseudo-capacitance that is modified by the electrode geometry, j an imaginary number, and P is an exponential parameter that expresses the electrode geometry as a number. Finally, $\omega = 2\pi f$ is the angular frequency and f is the frequency of the applied AC signal.

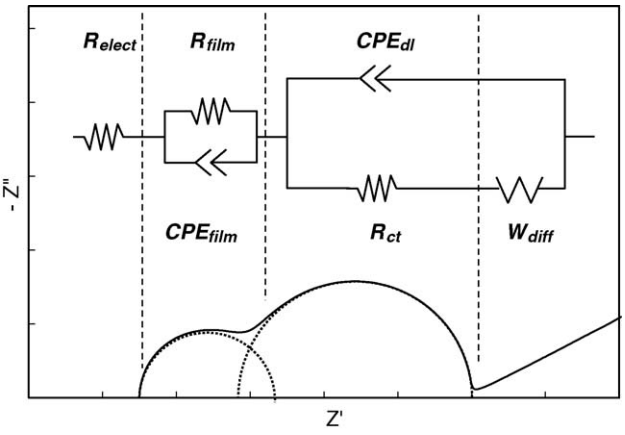

Fig. 2. Equivalent circuit for graphite/polysiloxane based electrolyte/lithium metal cell.

As described previously [1], two kinds of passive films were generated on a graphite particle during the first charge in the polysiloxane-based electrolyte. An island-like film was generated on the graphite surface in the range of 1.7–2.2 V versus Li/Li$^+$, followed by the formation of a gel-like film on the island-like film in the 1.2–1.7 V range. An EC was constructed based not only on the electrochemical features of the passive films and the reaction at the electrolyte-graphite junction, but also on the geometrical features of the graphite surface as observed by SEM [1,44,48,49].

The EC proposed in this study contains the resistance element, R_{elect}, representing the resistance of the bulk electrolyte, and an *R*–CPE parallel circuit [37–42,50,51] for the gel-like film and the island-like film with resistance R_{film} and constant phase element, CPE_{film} (Fig. 2). The other component is an *R*–CPE parallel [52] element that includes the electric double-layer capacitance represented by CPE_{dl} and the charge transfer resistance, R_{ct}, for the site where an electrochemical reaction occurs. Each CPE contains the pseudo-capacitance and exponential parameter, as expressed in Eq. (1), i.e., T_{film} and P_{film} for CPE_{film}, and T_{dl} and P_{dl} for CPE_{dl}, respectively. The diffusion impedance $W_{s,\,diff}$ is connected in series to R_{ct} [46,53–55]. For the EC element representing the lithium movement in both films and the electrochemical reaction at the junction of graphite and electrolyte, a CPE was used in a parallel circuit coupled with a resistance to describe these geometrical features mathematically.

4. Results

4.1. SEM images and AES compositional analysis results

SEM images of pristine HOPG and HOPG samples charged at 2.0 V, 1.6 V, 1.4 V, and 0.02 V versus Li/Li$^+$ are shown in Fig. 3(a–e), respectively. The pristine HOPG showed clear basal and edge surface planes (Fig. 3(a)). An island-like film was observed on the surface of the basal plane at 2.0 V (Fig. 3(b)). For HOPGs charged at 2.0 V, 1.8 V, and 1.7 V, the gel-like film

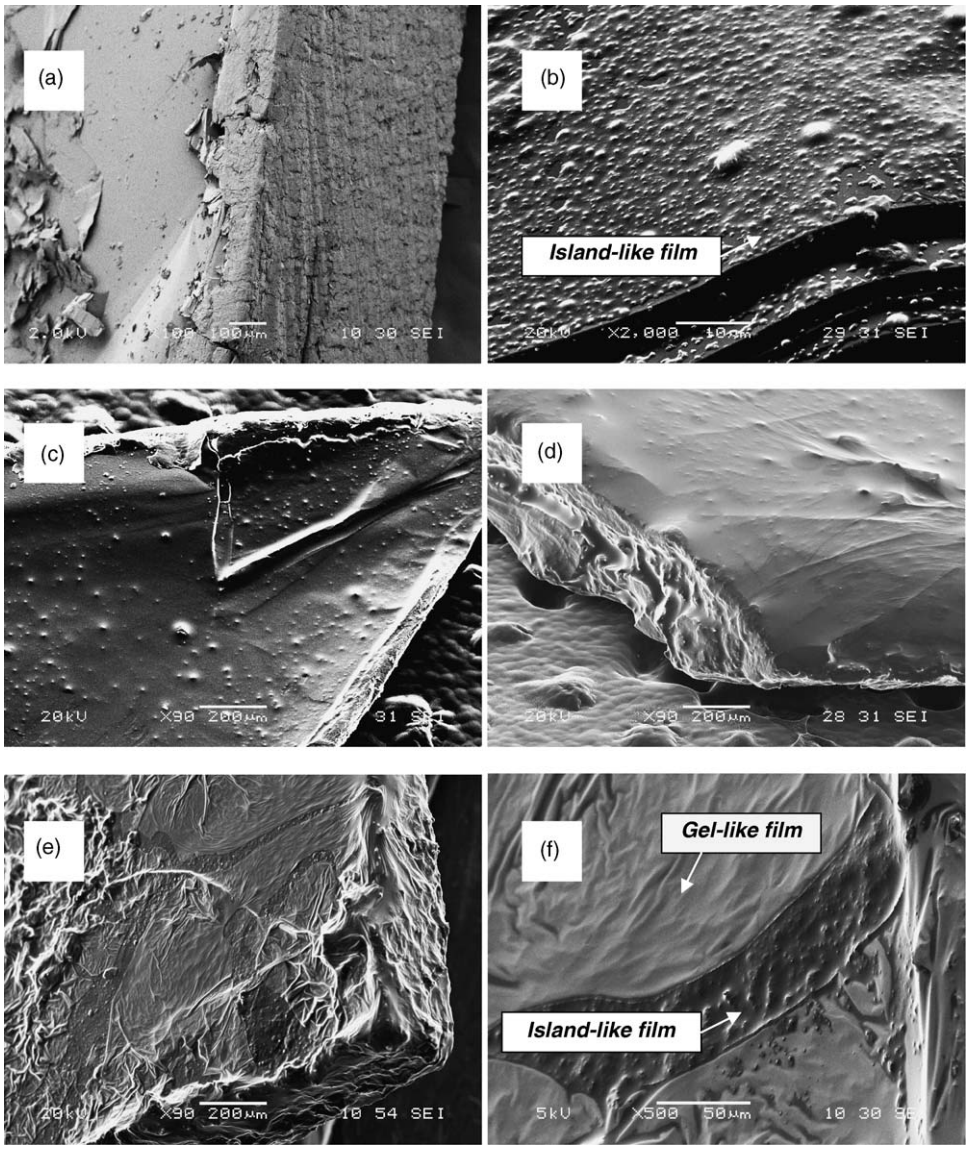

Fig. 3. SEM images of HOPG block charged at (a) 3.2 V, (b) 2.0 V, (c) 1.6 V, (d) 1.4 V, (e) 0.02 V vs. Li/Li^+ taken from ref. [1]. The island-like film can be observed through the rupture of gel-like film covering the entire HOPG (f) and the HOPG surface at 2.0 V (e).

was not observed in SEM images. A gel-like film was observed on the basal plane at 1.6 V (Fig. 3(d)). With a decrease in cell voltage from 1.6 V (Fig. 3(d)) to 0.02 V (Fig. 3(e)), the gel-like film covered the entire HOPG progressively. The HOPG block was covered by the gel-like film completely at 1.0 V. In addition, some ruptures were observed in the gel-like film (Fig. 3(e)). Within the ruptured region, an island-like film can be observed (Fig. 3(f)).

A set of depth profiles, from AES spectra of the HOPG surface charged at 0.02 V (gel-like film portion), is shown in Fig. 4. Fig. 4(a) shows an AES depth profile after sputtering for 125 min. Silicon, oxygen, carbon, boron, and lithium were detected in the deposited materials. The concentration of oxygen decreased with increasing depth beneath the surface, whereas the concentration of carbon increased. The deposited layers were largely removed after 80 min of sputtering because carbon was found to be the only dominant element. The concentration of lithium, boron, and silicon are relatively unchanged and are essentially negligible in this time scale. The 20-min depth profiles of AES spectra are shown in Fig. 4(b) to detect near-surface atomic components. In this time range of sputtering, the discontinuous nature of the atomic composition can be observed for all detected atoms. The concentration of lithium and silicon is relatively high for the 5-min region during the beginning of sputtering, that is, near the surface only. Carbon and oxygen are the dominant components in the deeper region, after sputtering for more than 10 min. The atomic composition of the island-like film in the rupture region (Fig. 3(f)) was also analyzed by AES (not shown). In island-like film region, carbon and oxygen were detected in composition profiles that were similar to that of Fig. 4(b) after more than 5 min of sputtering. Silicon and boron were not detected.

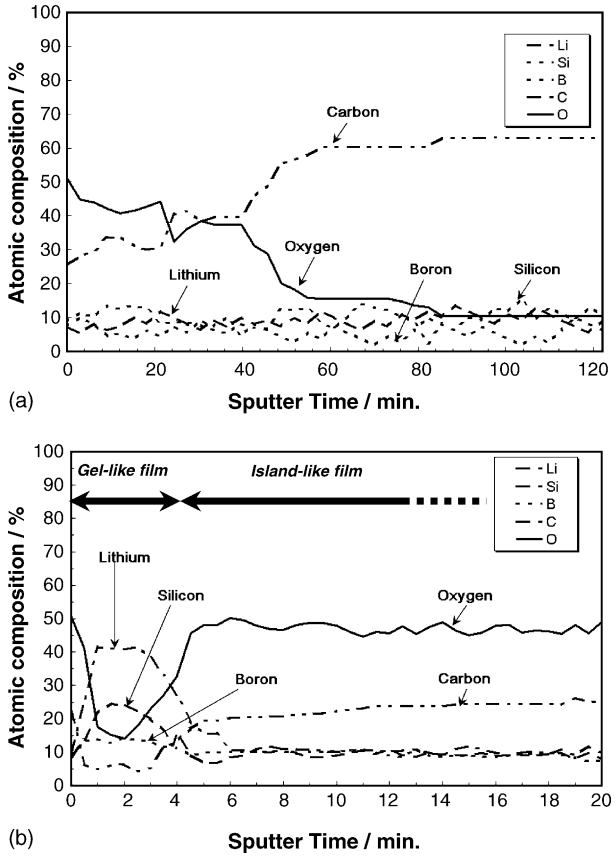

Fig. 4. AES spectra of the surface of the HOPG charged at 0.02 V taken under Ar-sputtering: (a) total sputtering time: 125 min, (b) total sputtering time: 20 min.

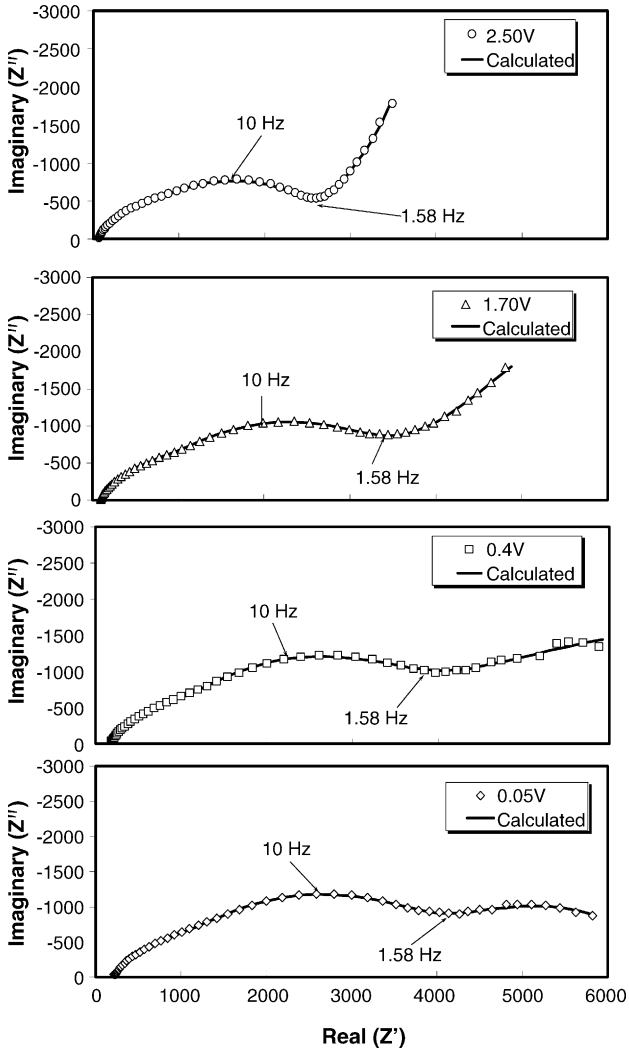

Fig. 5. Nyquist plots for graphite/polysiloxane based electrolyte/lithium metal cell measured at 2.5 V, 1.7 V, 0.4 V, and 0.05 V vs. Li/Li^+.

4.2. EIS results

The EIS data measured at 2.5 V, 1.7 V, 0.4 V, and 0.05 V are shown in Fig. 5. The semicircles in the complex plane plots are depressed. The semicircle in the mid- or low-frequency region became significantly broader as the cell voltage was decreased. The slope of the line in the low-frequency region decreased with decreasing cell voltage in the high-voltage domain (above 0.5 V). As the applied voltage was decreased below 0.5 V, the straight line in the low-frequency region disappeared and an additional semicircle was detected.

Fig. 6 shows the Bode plots corresponding to the complex plane plots in Fig. 5. The upper figure (Fig. 6a) shows the logarithm of the measured impedance modulus, $|Z|$ plotted against the logarithm of applied frequency. $|Z|$ decreased with a decrease in cell voltage between 1.8 V and 3.2 V over the entire frequency range and increased with a decrease in cell voltage between 0.05 V and 1.8 V. The lower figure (Fig. 6b) shows the phase angle of the measured impedance as a function of the logarithm of the applied frequency. The phase angle decreased with lower cell voltage at 1 kHz.

Superimposed on the experimental data in Figs. 5 and 6 are the fitted curves based on the EC in Fig. 2. The mean square deviation, χ^2, representing the sum of squared distances between the experimental and calculated spectra in the complex plane, was less than 1.22×10^{-4}, which is substantially less than values reported previously [27,40]. The relative standard deviation for all parameters obtained from calculations was less than 15%.

The values of all impedance elements of the equivalent circuit depend on the cell voltage. For example, consider the conductivity, which is plotted versus potential in Fig. 7. The conductivity was derived using the experimental value of R_{elect}. While the electrolyte conductivity did not change appreciably between 2.1 V and 3.2 V, it decreased sharply with decreasing cell voltage between 1.6 V and 1.9 V, and then more gradually in the regions of 1.05–1.2 V and 0.3–0.5 V.

The circuit parameters corresponding to the formation of the island-like film and the gel-like film were evaluated to clarify the dependence of these parameters on cell voltage. The dependence of R_{film} on cell voltage is shown in Fig. 8, and the dependence of T_{film} on cell voltage is shown in Fig. 9. R_{film} was constant at voltages above 1.8 V, increased gradually between 0.2 V and 1.8 V, and then decreased below 0.2 V. Close inspection of the data in Fig. 8 reveals that two plateau regions appear at cell voltages of 1.2–1.7 V and 0.6–1 V. The T_{film} values plotted in Fig. 9 show the same dependence on R_{film} at voltages above

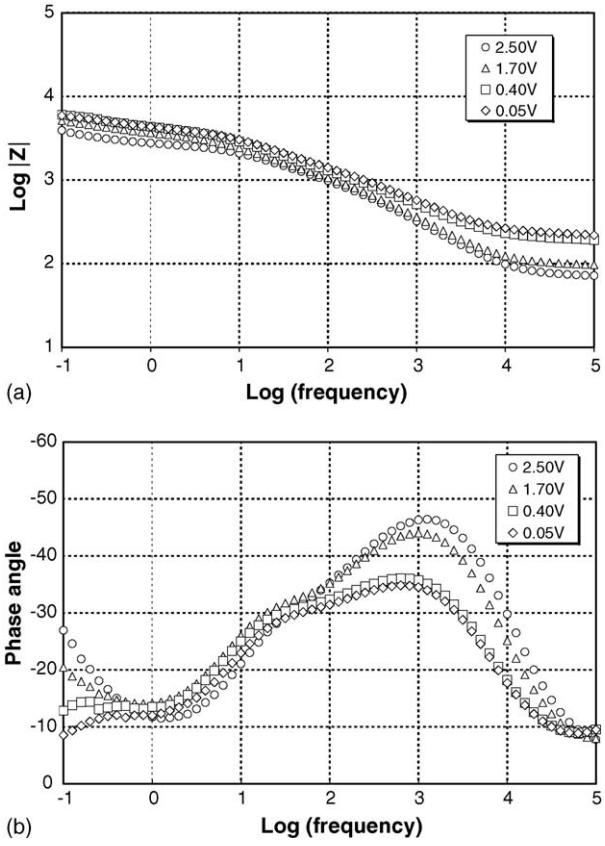

Fig. 6. Bode plots for graphite/polysiloxane based electrolyte/lithium metal cell measured at 2.5 V, 1.7 V, 0.4 V, and 0.05 V vs. Li/Li$^+$.

0.6 V. At cell voltages below 0.6 V, the T_{film} values decrease with decreasing cell voltage.

The dependence of the double-layer capacitance parameter, T_{dl} on cell voltage is shown in Fig. 10. Although the value of T_{dl} did not change above 1.75 V, it decreased with decreasing cell voltage below 1.75 V. The charge transfer resistance, R_{ct}, was approximately constant above 1.9 V, but increased with decreasing cell voltage below 1.9 V (Fig. 11).

The maximum and minimum values of each parameter are shown in Table 1 in order to clarify the dominant parameter in the impedance of the system. Among resistance elements, the

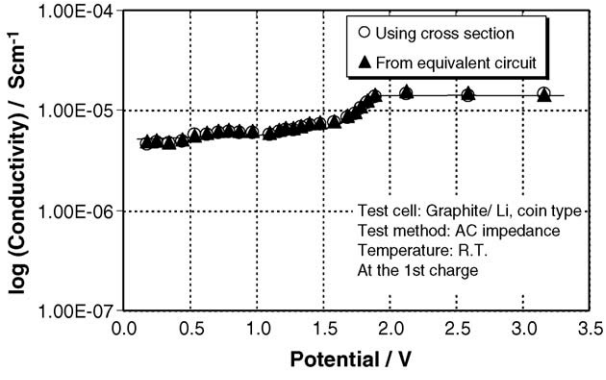

Fig. 7. The calculated conductivity of the electrolyte as a function of the cell voltage.

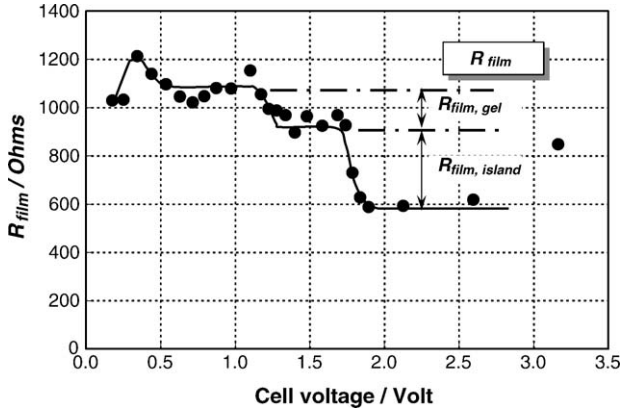

Fig. 8. The parameter values of R_{film} as a function of the voltage of graphite/polysiloxane based electrolyte/lithium metal cell.

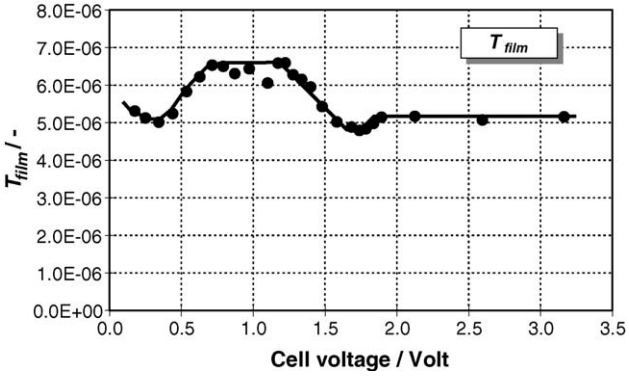

Fig. 9. The parameter values of T_{film} as a function of the voltage of graphite/polysiloxane based electrolyte/lithium metal cell.

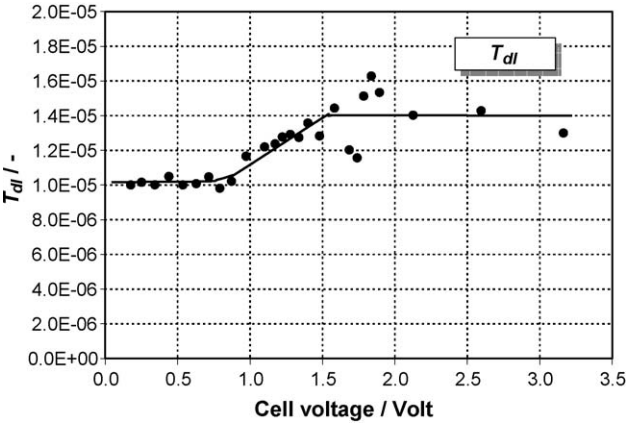

Fig. 10. The parameter values of T_{dl} as a function of the voltage of graphite/polysiloxane based electrolyte/lithium metal cell.

Table 1
The maximum and minimum value for the each parameter in the equivalent circuit

	R_{elect} (Ω)	R_{film} (Ω)	T_{film} (F)	T_{dl} (F)	R_{ct} (Ω)
Maximum	209.8	1214	4.79×10^{-5}	1.63×10^{-5}	4180
Minimum	62.46	587.7	6.59×10^{-6}	9.82×10^{-6}	2168

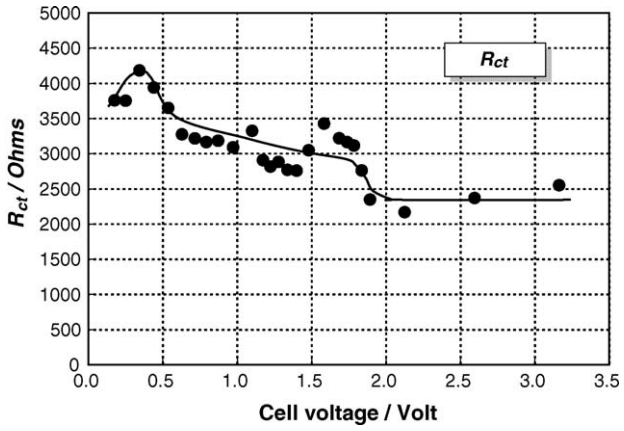

Fig. 11. The parameter values of R_{ct} as a function of the voltage of graphite/polysiloxane based electrolyte/lithium metal cell.

charge transfer resistance, R_{ct} was the largest, while the largest capacitance was the double-layer capacitance T_{dl}.

5. Discussion

5.1. Morphological and compositional analysis

SEM observations of HOPG surfaces revealed a sequential passive film formation with decreasing voltage. An island-like film deposited on the HOPG surface initially, and this was followed by gel-like film formation. In addition, the morphology of the island-like film was preserved after gel-like film formation, and this was interpreted as two passive film layers on the HOPG surface.

Based on the AES spectra, there were apparently two layers having different compositions. Fig. 4(b) indicated that the near-surface layer was composed of lithium and silicon as main atoms. Silicon is one component of the polysiloxane molecule, and the near-surface layer (gel-like film) is produced by the decomposition of polysiloxane molecules. In addition, carbon and oxygen were also detected in a subsurface layer, indicating that the island-like film was produced by decomposition of bis(oxalato)anions. Closer inspection revealed that the near-surface layer contained boron, indicating that decomposition of bis(oxalato)anions plays a role in the formation of both the gel-like film the island-like film. These AES results are consistent with electrochemical properties and SEM observations that reveal the existence of two layers—an island-like layer and a gel-like film layer covering the entire HOPG.

5.2. Verification of the proposed equivalent circuit

Fig. 5 shows that the curve calculated using the fit parameters from the proposed EC closely matches the experimental data. The small uncertainty, χ^2, of the fitting results supports the assertion that the proposed EC (Fig. 2) is suitable for modeling the electrochemical reactions in the graphite/polysiloxane based electrolyte/lithium metal cell system. The EC thus constitutes a reliable analog representing the electrochemical properties of the passive films and the electrochemical reaction on the graphite surface.

5.3. Relationship between morphological/compositional and EIS analyses

The pronounced changes in R_{film} and T_{film} that occur at cell voltages between 1 V and 2 V (Figs. 8 and 9) indicate the formation of surface films on the graphite electrode as reported previously [1]. The formation of the island-like film and the gel-like film results in higher resistivity than that of the fresh polysiloxane-based electrolyte.

The continuous increase in R_{film} indicates that either the island-like film becomes thicker as the cell voltage is decreased below 1.9 V, or the number of deposited islands increases, providing resistive obstacles against the lithium intercalation reaction on the graphite surface. In addition, the increase of T_{film} indicates the formation of a porous or rough film with increased surface area because the capacitance is proportional to the surface area of the boundary of two different materials [37]. This consideration is also supported by the observed growth of the island-like film and the gel-like film [1].

Based on the observed increase in resistance and decrease in capacitance, it appears that the island-like film becomes a homogeneous and solid film as the cell voltage is decreased between 0.3 V and 0.7 V. In the voltage region below 0.3 V, the graphite volume expands with lithium intercalation which may cause disruptions in the island-like film. However, the film is immediately regenerated where the graphite surface is exposed to the electrolyte. This process causes the surface area of the film to increase, thereby increasing the capacitance and decreasing the resistance as observed in the cell voltage region below 0.3 V.

The formation of the gel-like film is strongly affected by the reaction that leads to the formation of the island-like film. This assertion is supported by the observed dependency of R_{film} and T_{film} for both films on cell voltage (Figs. 8 and 9). The observed dependency is consistent with SEM observations and AES compositional analysis of film morphology and compositional analysis of the films (Figs. 3 and 4) [1].

Recent reports have indicated that cross-links can be initiated in the polysiloxane containing lithium bis(allylmalonato)borate salt by the decomposition of bis(allylmalonato)borate anions producing a larger molecule [56–61]. The previous reports [8–10,62] indicate that the reduction decomposition of LiBOB salt on the surface of graphite during the first charge can trigger the formation of the island-like film. In addition, the by-product may behave as an initiator or catalyst for the formation of the gel-like film with the polysiloxane molecules [1,56,60–62]. AES analysis of the near-surface layer further supports this assertion. The network frame of the macro-sized polysiloxane molecules initiated by LiBOB decomposition can accommodate and incorporate the polysiloxane-based electrolyte, which forms a gel-like interpenetrating polymer electrolyte [14,15].

Examination of Fig. 7 reveals plateaus at 1.3–1.7 V and at 0.7–1.2 V. The resistance values at those plateaus correspond to the formation of the island-like film ($R_{film,\ island}$) and the gel-like film ($R_{film,\ gel}$), respectively. $R_{film,\ gel}$ was estimated to be

about 200 Ω based on the data in Fig. 8, which was similar to the electrolyte resistance (210 Ω). The values of R_{elect} and $R_{film,\ gel}$ were similar because lithium ions can migrate at equal rates in the gel-like film and in the original polysiloxane-based electrolyte. Furthermore, because the macro-sized polysiloxane is capable of lithium ion transport [56,60,61], it is not surprising that the resistivity of the gel-like film is essentially the same as that of the fresh polysiloxane-based electrolyte, as shown in Table 1.

5.4. Electric double-layer capacitance and charge transfer resistance

The increase of R_{ct} and the decrease of T_{dl} with cell voltage between 0.3 V and 1.8 V indicate a decrease in the surface contact area available for the electrochemical reaction between the graphite surface and the electrolyte. In addition, the island-like film may inhibit the charge transfer reaction on the graphite surface. As a result, the dependence of R_{ct} and T_{dl} on cell voltage shows that the graphite surface is completely covered by the island-like film at 0.3 V.

The measured dependence of the charge transfer resistance, R_{ct} on cell voltage is consistent with previous reports [27,40,44]. However, the *range* of the absolute value is substantially different in this study, where $R_{ct} = 3797–7418\ \Omega\,cm^2$. For the gel polymer system [27] comprised of PEGDMA-MMA/carbonate dissolving $LiPF_6$ electrolyte, the R_{ct} value was reportedly $1–2800\ \Omega\,cm^2$; while for the carbonate solvent containing dissolved $LiPF_6$ [40] R_{ct} was $3–10\ \Omega\,cm^2$ and for the carbonate solvent dissolving $LiClO_4$ [44] R_{ct} was $60–80\ \Omega\,cm^2$. Comparing these R_{ct} values, R_{ct} for the polysiloxane-based electrolyte is significantly greater. However, the electric double-layer capacitance, T_{dl} falls in the same range of values observed in other studies [27]. The value of the passive film resistance R_{film} is two orders of magnitude larger than previously reported values [27,40] although the capacitance values T_{film} fall in the same range or less. As a result, the increase in cell impedance is attributed primarily to the formation of the island-like film on the graphite surface because the resistivity of the island-like film is greater than that of the gel-like film, as discussed above.

5.5. Conductivity of electrolyte

Several factors are considered which might cause the conductivity of the bulk electrolyte to decrease and these factors may not be mutually exclusive. The conductivity calculated from the EIS results includes the electrolyte bulk conductivity and the electric contact conductivity among the components in the test cell. Consequently, based on the above discussion of passive film formation, the observed conductivity change reflects the change in the electric contact resistance among graphite particles due to the passive film formations because the voltage at which the conductivity decreased corresponds to passive film formation. An assessment of the relative contributions of these factors is beyond the scope of the present work and awaits further study.

6. Conclusions

Two types of passive films with distinct compositions formed on the surface of graphite charged in polysiloxane-based electrolyte, and the graphite electrode exhibited distinct electrical properties. The proposed EC accurately expressed the electrochemical reaction occurring as well as the electrical properties of the passive films present on the graphite surface. The charge transfer resistance and the film resistance were the critical electrochemical properties controlling the behavior of the graphite electrode in the lithium battery system studied.

The present work has shown how the electrochemical characteristics of the graphite electrode are related to SEI film formation. The findings indicate a means for preventing the formation of the gel-like and island-like films on the electrodes, and may lead to the breakthrough needed to achieve superior electrochemical properties of the graphite electrode used in polysiloxane-based electrolyte. It has been shown that the modification of the graphite surface can improve high-rate discharge capability, calendar life and cycle life of a lithium rechargeable cell with polysiloxane-based electrolyte.

The use of an additive to the polysiloxane-based electrolyte prevented the formation of the gel-like film and produced an increase in the discharge capacity of the graphite electrode [1]. In addition to the intrinsic electric properties of the gel-like film, the additive modified the graphite surface covered with the island-like film and inhibited formation of gel-like films. As a consequence, the additive may reduce the charge transfer resistance and the film resistance for the battery system studied. Polysiloxane-based electrolyte with suitable additives for surface modification will further clarify the nature and formation mechanisms of passive films.

Acknowledgements

The support for this study from the US Army Communications-Electronics Command Center (CECOM), University of Wisconsin, and Argonne National Laboratory is gratefully acknowledged.

References

[1] H. Nakahara, A. Masias, S.Y. Yoon, T. Koike, K. Takeya, Proceedings of the 41st Power Sources Conference in Philadelphia, 14–17 June, 2004, p. 165.
[2] M. Inaba, Z. Shiroya, Y. Kawatate, A. Funabiki, Z. Ogumi, J. Power Sources 68 (2) (1997) 221–226.
[3] S.-K. Jeong, M. Inaba, Y. Iriyama, T. Abe, Z. Ogumi, Electrochim. Acta 47 (2002) 1975–1982.
[4] R. Mogi, M. Inaba, Y. Iriyama, T. Abe, Z. Ogumi, J. Power Sources 108 (2002) 163–173.
[5] D. Aurbach, E. Zinigrad, Y. Cohen, H. Teller, Solid State Ionics 148 (2002) 405–416.
[6] D. Aurbach, I. Weissman, A. Zaban, P. Dan, Electrochim. Acta 45 (1999) 1135–1140.
[7] D. Aurbach, A. Zaban, Y. Gofer, Y.E. Ely, I. Weissman, O. Chusid, O. Abramson, J. Power Sources 54 (1995) 76–84.
[8] Z. Ogumi, A. Sano, M. Inaba, T. Abe, J. Power Sources 97–98 (2001) 156–158.

[9] K. Xu, S. Zhang, B.A. Poese, T.R. Jow, Electrochem. Solid-State Lett. 5 (11) (2002) A259–A262.
[10] K. Xu, S. Zhang, T.R. Jow, W. Xu, C.A. Angell, Electrochem. Solid-State Lett. 5 (1) (2002) A26–A29.
[11] K. Xu, S. Zhang, T.R. Jow, Electrochem. Solid-State Lett. 6 (6) (2003) A117–A120.
[12] Y. Kang, W. Lee, D.H. Suh, C. Lee, J. Power Sources 119–121 (2003) 448–453.
[13] I.J. Lee, G.S. Song, W.S. Lee, C. Lee, J. Power Sources 114 (2003) 320–329.
[14] M. Shibata, T. Kobayashi, R. Yosomiya, M. Seki, Eur. Polym. J. 36 (2000) 485–490.
[15] Z. Zhang, S. Fang, Electrochim. Acta 45 (2000) 2131–2138.
[16] Z. Wang, M. Ikeda, N. Hirata, M. Kubo, T. Ito, O. Yamamoto, J. Electrochem. Soc. 146 (6) (1999) 2209–2215.
[17] B. Oh, D. Vissers, Z. Zhang, R. West, H. Tsukamoto, K. Amine, J. Power Sources 119–121 (2003) 442–447.
[18] N. Hiroyoshi, S. Kuroiwa, H. Miki, M. Tsunekawa, T. Hirajima, Hydrometallurgy 74 (2004) 193.
[19] K. Abe, H. Yoshitake, T. Kitakura, T. Hattori, H. Wang, M. Yoshio, Electrochim. Acta 49 (26) (2004) 4613.
[20] M.-S. Wu, P.-C.J. Chiang, J.-C. Lin, J.-T. Lee, Electrochim. Acta 49 (2004) 4379.
[21] M.S. Michael, S.R.S. Prabaharan, J. Power Sources 136 (2004) 250.
[22] S.-H. Choi, J. Kim, Y.-S. Yoon, Electrochim. Acta 50 (2–3) (2004) 547.
[23] C.H. Chen, J. Liu, M.E. Stoll, G. Henriksen, D.R. Vissers, K. Amine, J. Power Sources 128 (2004) 278.
[24] J.-H. Kim, C.W. Park, Y.-K. Sun, Solid State Ionics 164 (2003) 43.
[25] Z.P. Guo, S. Zhong, G.X. Wang, H.K. Liu, S.X. Dou, J. Alloys Compd. 348 (2003) 231.
[26] S.S. Zhang, T.R. Jow, J. Power Sources 109 (2002) 458.
[27] S. Zhang, P. Shi, Electrochim. Acta 49 (2004) 1475.
[28] Z. Ogumi, T. Abe, T. Fukutsuka, S. Yamate, Y. Iriyama, J. Power Sources 127 (2004) 72.
[29] S. Komaba, T. Itabashi, B. Kaplan, H. Groult, N. Kumagai, Electrochem. Commun. 5 (2003) 962.
[30] J. Yao, G.X. Wang, J.-H. Ahn, H.K. Liu, S.X. Dou, J. Power Sources 114 (2004) 292.
[31] M. Nookala, B. Kumar, S. Rodrigues, J. Power Sources 111 (2002) 165.
[32] Y.-K. Choi, K.-I. Chung, W.-S. Kim, Y.-E. Sung, S.-M. Park, J. Power Sources 104 (2002) 132.
[33] S.B. Lee, S.-I. Pyun, Carbon 40 (2002) 2333.
[34] F. Kong, F. McLarnon, J. Power Sources 89 (2000) 180.
[35] C.S. Wang, A.J. Appleby, F.E. Little, Electrochim. Acta 46 (2001) 1793.
[36] B. Jin, J.-U. Kim, H.-B. Gu, J. Power Sources 117 (2003) 148.
[37] C.R. Yang, J.Y. Song, Y.Y. Wang, C.C. Wan, J. Appl. Electrochem. 30 (2000) 29.
[38] Y.C. Chang, J.H. Jong, G.T.K. Fey, J. Electrochem. Soc. 147 (2000) 2033.
[39] Y.C. Chang, H.J. Sohn, J. Electrochem. Soc. 147 (2000) 50.
[40] M. Holzapfel, A. Martinent, F. Alloin, B. Le Gorrec, R. Yazami, C. Montella, J. Electroanal. Chem. 546 (2003) 41.
[41] T. Piao, S.M. Park, C.H. Doh, S.I. Moon, J. Electrochem. Soc. 146 (1999) 2794.
[42] F. Prieto, I. Navarro, M. Rueda, J. Electroanal. Chem. 550–551 (2003) 253.
[43] N. Hiroyoshi, S. Kuroiwa, H. Miki, M. Tsunekawa, T. Hirajima, Hydrometallurgy 74 (2004) 193.
[44] S. Yoon, H. Kim, S.-M. Oh, J. Power Sources 94 (2001) 68.
[45] J.R. MacDonald, W.R. Kenan, Impedance Spectroscopy: Emphasizing Solid Materials and Systems, John Wiley & Sons, New York, 1987.
[46] J. Bisquert, A. Compte, J. Electroanal. Chem. 499 (2001) 112.
[47] Y.O. Kim, S.M. Park, J. Electrochem. Soc. 148 (2001) A194.
[48] E. Basrsoukov, J.H. Kim, C.H. Yoon, H. Lee, J. Electrochem. Soc. 145 (1998) 2711.
[49] J.-S. Kim, Y.-T. Park, J. Power Sources 91 (2000) 172.
[50] M.W. Wagner, Electrochim. Acta 10 (1997) 1623.
[51] V. Doge, J. Dreher, G. Hambitzer, IEEE 0-7803-2459-5/95 (1995).
[52] S. Buller, M. Thele, R.W. De Doncker, IEEE 0-7803-0/03 (2003).
[53] I. Uchida, M. Mohamedi, K. Dokko, M. Nishizawa, T. Itoh, M. Umeda, J. Power Sources 97–98 (2001) 518.
[54] R.M. Spotnitz, IEEE 0-7803-5924-0/00 (2000).
[55] M.J. Issacson, N.A. Torigoe, R.P. Hollandsworth, IEEE 0-7803-4098-1/98 (1998).
[56] X.G. Sun, J.B. Kerr, C.L. Reeder, G. Liu, Y. Han, Macromolecules 37 (14) (2004) 5133.
[57] S. Bayoudh, N. Parizel, L. Reibel, Polym. Int. 49 (2000) 703.
[58] J.F. Snyder, M.A. Ratner, D.F. Shriver, J. Electrochem. Soc. 150 (8) (2003) A1090.
[59] M. Doyle, L. Wang, Z. Yang, S.K. Choi, J. Electrochem. Soc. 150 (11) (2003) D185.
[60] W. Xu, C.A. Angell, Solid State Ionics 147 (2002) 295.
[61] X.G. Sun, C.L. Reeder, J.B. Kerr, Macromolecules 37 (2004) 2219.
[62] K. Xu, U. Lee, S. Zhang, J.L. Allen, T.R. Jow, Electrochem. Solid-State Lett. 7 (9) (2004) A273.